BIOLOGICAL CRYSTALLOGRAPHY
ISSN 1399-0047

Atomic resolution crystal structure of Sapp2p, a secreted aspartic protease from *Candida parapsilosis*

Jiří Dostál,[a,b]* Adam Pecina,[a,b] Olga Hrušková-Heidingsfeldová,[a,b] Lucie Marečková,[a] Iva Pichová,[a,b] Pavlina Řezáčová,[a,c] Martin Lepšík[a,b] and Jiří Brynda[a,c]*

[a]Institute of Organic Chemistry and Biochemistry (IOCB), Academy of Sciences of the Czech Republic, Flemingovo náměstí 2, 166 10 Prague 6, Czech Republic, [b]Gilead Sciences and IOCB Research Centre, Flemingovo náměstí 2, 166 10 Prague 6, Czech Republic, and [c]Institute of Molecular Genetics, Academy of Sciences of the Czech Republic v.v.i., Vídeňská 1083, 142 20 Prague 6, Czech Republic. *Correspondence e-mail: dostalj@uochb.cas.cz, brynda@uochb.cas.cz

Received 2 September 2015
Accepted 13 October 2015

Edited by Z. Dauter, Argonne National Laboratory, USA

Keywords: aspartic protease; *Candida parapsilosis*; Sapp2p; crystal structure; ultrahigh resolution; interaction energy; quantum mechanics.

PDB reference: Sapp2p, 4y9w

Supporting information: this article has supporting information at journals.iucr.org/d

The virulence of the *Candida* pathogens is enhanced by the production of secreted aspartic proteases, which therefore represent possible targets for drug design. Here, the crystal structure of the secreted aspartic protease Sapp2p from *Candida parapsilosis* was determined. Sapp2p was isolated from its natural source and crystallized in complex with pepstatin A, a classical aspartic protease inhibitor. The atomic resolution of 0.83 Å allowed the protonation states of the active-site residues to be inferred. A detailed comparison of the structure of Sapp2p with the structure of Sapp1p, the most abundant *C. parapsilosis* secreted aspartic protease, was performed. The analysis, which included advanced quantum-chemical interaction-energy calculations, uncovered molecular details that allowed the experimentally observed equipotent inhibition of both isoenzymes by pepstatin A to be rationalized.

1. Introduction

Candida parapsilosis is an opportunistic fungal pathogen. Although it is less common and less virulent than *C. albicans*, it causes a wide variety of hospital-acquired infections and presents a serious problem, particularly in neonatal intensive-care units (Leibovitz *et al.*, 2013; Pammi *et al.*, 2013; Trofa *et al.*, 2008). *C. parapsilosis* is an exogenous pathogen that often forms biofilms on catheters and other inserted devices, and it has been isolated from the hands of healthcare workers more frequently than other yeast species (Pammi *et al.*, 2013; Pfaller *et al.*, 2010). *C. parapsilosis* has also been isolated from a variety of natural sources, including soil, insects and domestic animals (Pryszcz *et al.*, 2013; Trofa *et al.*, 2008).

The success of pathogenic *Candida* species in colonizing and infecting various host niches relies on several specific features, such as efficient adherence to host surfaces, morphological diversity, biofilm formation, adaptability of metabolism and secretion of hydrolytic enzymes. The extracellular hydrolases, namely aspartic proteases, lipases and phospholipases, facilitate the penetration of the pathogens through host tissues. Secreted aspartic proteases (Saps) of pathogenic *Candida* spp. have broad substrate specificities and degrade a wide variety of host protein substrates ranging from structural proteins to immunoglobulins (Hrušková-Heidingsfeldová, 2008; Hube & Naglik, 2001). *SAP* genes usually occur

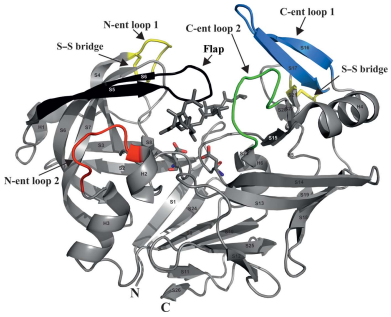

in gene families, which enables differential regulation according to ambient conditions and the stage of infection (Naglik *et al.*, 2004). The properties, regulation and evolution of the *SAP* gene family have been extensively studied, particularly in *C. albicans*, which possesses ten Sap isoenzymes. Four of the *C. albicans* Saps have been crystallized and structurally characterized (Abad-Zapatero *et al.*, 1996; Borelli *et al.*, 2007, 2008; Cutfield *et al.*, 1995). *C. parapsilosis* has long been considered to have only three genes encoding Saps. However, sequencing of the full *C. parapsilosis* genome enabled an *in silico* analysis that revealed up to 14 potential Sap-encoding sequences (Parra-Ortega *et al.*, 2009). This raised questions about the regulation of the individual *SAPP* genes and the properties of the putative protease isoenzymes.

Characterization of the first *C. parapsilosis* isoenzyme, Sapp1p, was facilitated by the fact that its expression can be induced by the presence of an exogenous protein as a sole source of nitrogen. Sufficient amounts of Sapp1p for crystallization can thus be easily obtained directly from *C. parapsilosis* culture supernatant. In our previous studies, we determined the crystal structures of Sapp1p in complex with pepstatin A, a classical aspartic protease inhibitor, and with ritonavir, a clinically used HIV protease inhibitor (Dostál *et al.*, 2009, 2012).

Expression of the second *C. parapsilosis* isoenzyme, Sapp2p, cannot be induced by a particular nitrogen source and its abundance is much lower than that of Sapp1p. When a protein is used as a source of nitrogen, Sapp2p usually constitutes less than 10% of the proteases recovered from the medium (Fusek *et al.*, 1993; Hrušková-Heidingsfeldová, 2008). In addition, two homologues of Sapp2p sharing 91.5% identity occur in the *C. parapsilosis* genome (Dostál *et al.*, 2015). Nevertheless, we succeeded in purifying and crystallizing one of the Sapp2p homologues, namely Sapp2p/CPAR2_102580 (entry CPAR2_102580 in the *Candida* Genome Database is identical to entry A47701 in the NCBI). Here, we report its structure in complex with pepstatin A determined at an atomic resolution of 0.825 Å. To understand the differences in pepstatin A binding to Sapp1p and Sapp2p on an accurate quantitative basis, we employed quantum-mechanical (QM) calculations to evaluate the interactions of the active-site residues with the inhibitor.

2. Materials and methods

2.1. Protein preparation

Sapp2p was purified from its natural source. *C. parapsilosis* strain P-69 was obtained from the mycological collection of the Faculty of Medicine, Palacky University, Olomouc, Czech Republic. The yeast was cultivated in YCB–BSA medium [1.2%(*w*/*v*) yeast carbon base, 0.2%(*w*/*v*) BSA, 15 m*M* sodium citrate pH 4.0] for 72 h at 303 K in a rotation shaker. The cells were harvested by centrifugation (5000*g* for 15 min). Isolation and purification of the mixture of Sapp2p and Sapp1p isoenzymes was performed as described in Hrušková-Heidingsfeldová *et al.* (2009) and Dostál *et al.* (2009). The efficiency of the purification steps was analyzed using SDS–PAGE, Western blotting and activity assays. Protein analyses and proteolytic activity assays were carried out as described previously (Pichová *et al.*, 2001; Dostál *et al.*, 2003; Merkerová *et al.*, 2006).

2.2. Mass-spectrometric analysis

Prior to identification by mass spectrometry (MS), proteins were separated using SDS–PAGE, stained with Coomassie Brilliant Blue R-250 (Thermo Scientific), excised from the gel and digested in-gel with either Trypsin Gold (Promega) or Endoproteinase Asp-N (Roche Applied Science). The resulting peptides were solubilized in 30 µl 0.1%(*w*/*v*) formic acid and injected into an Ultimate 3000 RSCL Nano LC (Thermo Scientific). The peptides were trapped on an Acclaim PepMap100 C18 trap column (3 µm particles, 100 Å, 75 µm × 2 cm; Thermo Scientific) and separated using an Acclaim PepMap RSCL C18 column (2 µm particles, 100 Å, 75 µm × 15 cm; Thermo Scientific). The mobile phase consisted of 0.1% formic acid in water (*A*) and 0.1% formic acid in acetonitrile (*B*) and the sample-loading solution consisted of 2% acetonitrile and 0.1% formic acid in water. All chemicals were Optima LC/MS grade (Thermo Scientific). The nano LC was coupled online with a TripleTOF 5600 system (AB Sciex). The MS scan was in the range *m*/*z* 350–1200 in high-resolution mode (>30 000) and the top 25 precursor ions were selected for subsequent MS/MS scans in high-sensitivity mode (>15 000). The data were processed using the *ProteinPilot* software 4.0 with the Paragon Algorithm 4.0.0.0 (AB Sciex). The software used only unique peptide sequences with greater than or equal to 95% confidence as evidence for protein identification. The data were searched against the UniProt database with the *BioWorks Browser* 3.3.1 SP1 and *SEQUEST* 2.0 software (Thermo Scientific). Only peptides identified with a confidence of ≥95% were taken into account.

2.3. Protein crystallization

The Sapp2p–pepstatin A complex was prepared by mixing the enzyme with a fivefold molar excess of pepstatin A (dissolved in dimethyl sulfoxide) and concentrated by ultrafiltration to 18 mg ml^{-1} using Amicon Ultra 0.5 ml 30K filters (Millipore). Screening for crystallization conditions was performed with the help of a Gryphon crystallization workstation (ArtRobbins) by the vapour-diffusion method in sitting-drop mode at 292 K in 96-well plates. The protein solution (0.2 µl) was mixed with 0.2 µl well solution and the mixture was equilibrated over 200 µl reservoir solution. The PEGs Suite (Qiagen) was used for the initial crystallization-condition screen. Initial microcrystals appeared in several days in various conditions containing 0.1 *M* MES pH 6.5 and 20–30% PEG 200–400 as precipitant.

Further optimization was performed manually and involved changing to the hanging-drop mode in 24-well crystallization plates (EasyXtal DG-Tool, Qiagen). Crystals were obtained by mixing 3 µl protein–pepstatin A complex solution with 1 µl reservoir solution composed of 0.1 *M* MES pH 6.5, 30% PEG

Table 1
Crystal data and diffraction data-collection and refinement statistics for the Sapp2p–pepstatin A complex.

For the data-collection statistics, the values in parentheses are for the highest resolution shell. For the refinement statistics, the values in parentheses are for reflections stronger then $4\sigma(F_o)$. The Friedel pairs were not merged in refinement.

Data-collection statistics	
Wavelength (Å)	0.91841
Space group	$P2_1$
Unit-cell parameters (Å, °)	a = 48.25, b = 57.58, c = 54.32, α = 90.0, β = 93.0, γ = 90.0
No. of molecules in asymmetric unit	1
Resolution range (Å)	12.820–0.825 (0.850–0.825)
No. of unique reflections	261700 (13705)
Multiplicity	8.1 (3.1)
Completeness (%)	92.3 (65.5)
R_{merge}†	0.087 (0.378)
Average $I/\sigma(I)$	13.2 (2.0)
Wilson B (Å^2)	6.2
Refinement statistics	
Resolution range (Å)	11.368–0.825
No. of reflections in working set	515542 (404510)
No. of reflections in test set	5199 (4050)
R_{work}‡ (%)	10.69 (9.32)
R_{free}§ (%)	13.15 (11.14)
R_{all} (%)	10.71 (9.33)
R.m.s.d., bond lengths (Å)	0.0217
R.m.s.d., bond angles¶ (Å)	0.0523
No. of non-H atoms in asymmetric unit	3044
No. of water molecules in asymmetric unit	393
Mean ADP (Å^2)	
Main chain	8.5
Side chain and water	14.0
Residues in alternative conformations	41
Ramachandran plot statistics	
Residues in favoured regions (%)	96.8
Residues in allowed regions (%)	2.5

† $R_{merge} = \sum_{hkl}\sum_i |I_i(hkl) - \langle I(hkl)\rangle| / \sum_{hkl}\sum_i I_i(hkl)$, where the average intensity $\langle I(hkl)\rangle$ is taken over all symmetry-equivalent measurements and $I_i(hkl)$ is the intensity of the ith measurement of reflection hkl. ‡ $R = \sum_{hkl} ||F_{obs}| - |F_{calc}|| / \sum_{hkl} |F_{obs}|$, where F_{obs} and F_{calc} are the observed and calculated structure factors, respectively. § R_{free} is equivalent to R but is calculated for 5% of the reflections that were chosen at random and omitted from the refinement process. ¶ Accurate bond angle is defined as the optimal distance between two atoms that are both bonded to the same atom.

400 and equilibrating the drop over 0.5 ml reservoir at 292 K. Crystals appeared after 1 d in the form of crystal clusters and reached their full size of 300 × 250 × 150 µm within 1 d. For data collection, the crystal was divided into three parts using a scalpel, and these were individually cryocooled in liquid nitrogen without additional cryoprotection.

2.4. Data collection and structure determination

The diffraction data set for the Sapp2p–pepstatin A complex was collected at 100 K on the MX14.2 beamline at BESSY, Berlin, Germany (Mueller *et al.*, 2012). Data were integrated, reduced and scaled with *XDS* (Kabsch, 2010) using the *xdsgui* interface (Diederichs, 2010). To collect as complete high-resolution data as possible, we merged and scaled data sets from two parts of the original crystal using *XSCALE* (Kabsch, 2010). The second part of the crystal was mounted in a different orientation to the first, and the merged data reached 92.3% completeness (65.5% for the highest shell); the mosaicity estimated by the program was 0.3° for both parts of the crystal. The low completeness at high resolution was caused by the physical limitations of the beamline at the closest distance of the detector. Moreover, for resolutions of up to 0.825 Å it was necessary to use diffraction spots in the corners of the MAR Mosaic 225 detector, and part of the detector area was shadowed by the cryodevice and beamstop support. Crystal parameters and data-collection statistics are given in Table 1.

The phase problem was solved by molecular replacement using *MOLREP* (Vagin & Teplyakov, 2010). The search model was derived from the structure of an Sapp1p–pepstatin A complex (PDB entry 3fv3; Dostál *et al.*, 2009). *MOLREP* found one molecule in the asymmetric unit using diffraction data in the resolution range 25.46–3.8 Å. The resulting R factor was 46.1%.

The model was rebuilt in *Coot* (Emsley & Cowtan, 2004) into the map calculated using phases from the molecular-replacement solution. This initial model of the Sapp2p–pepstatin A complex was submitted to *REFMAC* for isotropic refinement. Further model refinement was carried out in *SHELXL*2013 (Gruene *et al.*, 2014) using isotropic and anisotropic refinement protocols. The default *SHELXL* restraints ISOR, SIMU and DELU were applied to the anisotropic atomic displacement parameters (ADPs). The H-atom positions were recalculated at every refinement cycle in idealized positions, and their isotropic ADPs were fixed at values 20% higher than the ADPs of their parent atoms. The occupancies of side chains adopting alternative conformations were refined with their sums constrained to unity. Finally, the occupancies of O atoms of the solvent water were also refined. If the occupancy parameter was refined to a value exceeding 0.95, it was fixed at an occupancy value of 1. Cycles of refinement were interspersed with visual inspection sessions using *Coot*, and if necessary the model was corrected manually, for example, by introducing alternative conformations of several side chains. After applying the conjugate-gradient least-squares (CGLS) minimization method, the last round of refinement was performed using the full-matrix least-squares option, with the parameter shifts damped to zero, to obtain reliable estimations of all refined and derived parameters of the model. The Friedel pairs were not merged for the *SHELXL* refinement; the command MERG 2 was used. The final model and the corresponding structure factors have been deposited in the PDB with identification code 4y9w.

2.5. Molecular modelling

The crystal structure of pepstatin A in complex with Sapp2p (resolution of 0.83 Å, PDB entry 4y9w; this work) was compared with that of pepstatin A in complex with Sapp1p (resolution of 1.85 Å, PDB entry 3fv3; Dostál *et al.*, 2009). For the latter complex, two conformations of pepstatin A were observed in the eight molecules present in the asymmetric unit (conformation I was found in chains *A*, *B*, *C*, *D* and *F*, and conformation II was found in chains *E*, *G* and *H*). Both conformations were considered in this study. For further computations, all water molecules and ions were omitted. Protonation of histidines was assigned based on visual

inspection of their surroundings (all His resides were monoprotonated on N^{ε}). The protein N-terminus and the side chains of lysines and arginines were positively charged, while the C-terminus and the side chains of glutamates and aspartates (with the exception of the catalytic dyad) were negatively charged to reflect the predominant state at the experimental pH of 6.5–7.0. The active site was treated according to the crystallographic findings from the Sapp2p–pepstatin A complex, *i.e.* Asp211 was monoprotonated on the $O^{\delta 2}$ atom and Asp32 was either deprotonated or monoprotonated on the $O^{\delta 1}$ atom. The inhibitors were protonated using *UCSF Chimera* (Pettersen *et al.*, 2004). The positions of the added H atoms were relaxed *in vacuo* using the *FIRE* algorithm (Bitzek *et al.*, 2006) followed by molecular dynamics-based simulated annealing (3 ps from 1700 to 0 K) using the Berendsen thermostat (Berendsen *et al.*, 1984) in the *SANDER* module of the *AMBER* 10 package (Case *et al.*, 2008). Similarly, amino-acid residues that were not well defined in the electron-density maps (Ala208, Asn252, Pro253, Thr279 and Asn281) were relaxed by annealing (3 ps from 300 to 0 K) using the Berendsen thermostat. Atomic charges for the inhibitors were obtained by the *RESP* procedure (Bayly *et al.*, 1993) at the HF/6-31G* level. The protein parameters were obtained from the ff03 force field (Duan *et al.*, 2003), while GAFF parameters were used for the ligands (Wang *et al.*, 2004).

2.6. Quantum-mechanical calculations

2.6.1. Setup. All four model complexes, Sapp2p–pepstatin A with Asp32 deprotonated or monoprotonated (see above) and Sapp1p–pepstatin A in conformations I and II, were optimized using the following setup. Only surroundings of the ligands within 8 Å (approximately 1560 atoms in total) were taken into account. Of these atoms, only atoms belonging to amino acids within 6 Å of the ligand (approximately 1200 atoms) were allowed to move. The energies and gradients were obtained by the semi-empirical quantum-mechanical (SQM) method PM6-D3H4 coupled with the COSMO implicit solvent model using the linear scaling method *MOZYME* in *MOPAC* (Lepšík *et al.*, 2013). The SQM optimizations were performed in several rounds until the energy and gradient convergence criteria (ΔE = 0.005 kcal mol^{-1}, maximum gradient of 1 kcal mol^{-1} Å^{-1}, root mean square of the gradient of 0.5 kcal mol^{-1} Å^{-1}) were met. Interaction 'free' energies ($\Delta G'_{\rm int}$) of all of the studied systems were determined on the whole optimized structures using the PM6-D3H4 method and the COSMO solvent model.

2.6.2. Interaction energies. The differential contribution of the amino acids in the active sites of Sapp1p and Sapp2p to pepstatin A binding was examined by 'virtual glycine scanning' (Pecina *et al.*, 2013), *i.e.* the interacting amino acids in the active site were substituted by glycine. The energy contributions of their side chains ($\Delta\Delta G'_{\rm int}$) were calculated as the difference between the original $\Delta G'_{\rm int}$ with the wild-type amino acid and the new $\Delta G'_{\rm int}$ with the mutated glycine residue. The $\Delta G'_{\rm int}$ values were obtained on the whole optimized structures as single-point energies at the PM6-D3H4/COSMO level (Lepšík *et al.*, 2013).

3. Results and discussion

3.1. Purification of Sapp2p

Sapp2p was purified from *C. parapsilosis* cultivation medium, where it was present along with large amounts of Sapp1p, as described previously (Fusek *et al.*, 1993; Merkerová *et al.*, 2006; Hrušková-Heidingsfeldová *et al.* (2009). Two *SAPP2* homologues occur in the *C. parapsilosis* genome. They share 91.5% identity and differ mainly in their C-terminal sequence (Dostál *et al.*, 2015). We purified Sapp2p/CPAR2_102580 (the standard and systematic name according to http://www.candidagenome.org), which is the shorter of the two Sapp2p molecular species, consisting of 395 amino acids.

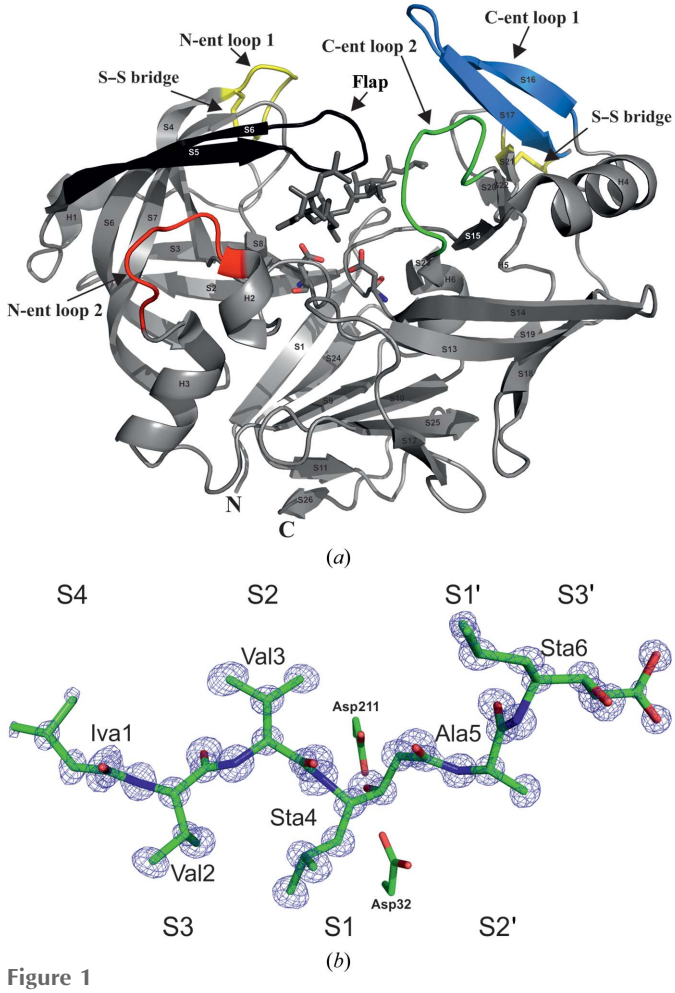

Figure 1
Overall structure of Sapp2p in complex with pepstatin A. (*a*) Overall three-dimensional structure and secondary-structural elements of Sapp2p in complex with pepstatin A. The protein is shown in ribbon representation; pepstatin A and the catalytic aspartates are shown in stick representation. The flap and entrance loops covering the active site are coloured and labelled. (*b*) Structure of pepstatin A bound to Sapp2p. The $2F_{\rm o} - F_{\rm c}$ electron-density map is contoured at 1.5σ. Residue names (Iva1-Val2-Val3-Sta4-Ala5-Sta6) and corresponding substrate-binding subsites (S4–S3′) are indicated. Catalytic aspartates are also shown as sticks.

Protein identity was confirmed by mass spectrometry. We did not detect any Sapp2p/P32950, and thus the question of the natural occurrence and role of this variant remains open.

3.2. Overall structure description and quality

The crystal structure of Sapp2p (Fig. 1) was solved by molecular replacement using the structure of Sapp1p (PDB entry 3fv3; Dostál *et al.*, 2009) as a search model and was refined to a resolution of 0.825 Å (Table 1). The crystal structure of Sapp2p in complex with pepstatin A belonged to space group $P2_1$, with a solvent content of 44%. The asymmetric unit contained one molecule of Sapp2p. All 395 residues could be modelled into the electron-density map, with the exception of the side chains of several surface-exposed residues (Ser33, Asn252, Pro253, Thr279, Ala208 and Asn281).

The Sapp2p structure comprises two topologically similar N- and C-terminal domains with a large substrate-binding cleft located between them (Fig. 1). The structure is stabilized by two disulfide bridges (Cys47–Cys52 and Cys249–Cys283). The conserved sequence DT(S)G, which is present as one copy in each domain and contains the catalytic aspartate residues (Asp32 and Asp211), is the signature motif of aspartic proteases (Rao *et al.*, 1991). Similar to other aspartic proteases, the Sapp2p active site is covered by an antiparallel β-sheet (residues 71–89), commonly known as the active-site flap, which plays an important role in substrate binding. Because the substrate-binding site in our structure is occupied by the substrate-mimicking inhibitor pepstatin A, the flap adopts a closed conformation. The substrate-binding site is lined by four entrance loops. Two N-terminal entrance loops, N-ent loop 1 (Cys47–Cys52) and N-ent loop 2 (Glu124–Asp132), flank the flap. Two C-terminal entrance loops, C-ent loop 1 (Ser289–Pro297) and C-ent loop 2 (Ala233–Ile247), are located across the binding cleft, facing the flap and the N-ent loop, respectively.

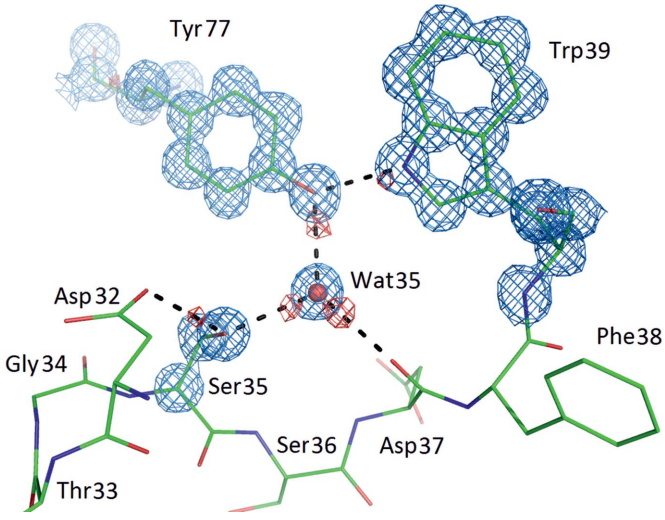

Figure 2
The network of hydrogen bonds stabilizing the closed flap. Detail of the hydrogen-bonding network between the flap and the catalytic site. The Tyr77 side chain and the stretch of amino-acid residues 32–39 are shown in stick representation; hydrogen bonds are shown as black dashed lines. The $2F_o - F_c$ electron-density map contoured at the 1.5σ level is shown in light blue and the $F_o - F_c$ difference electron-density map contoured at the 1.8σ level is shown in red. Both maps are calculated from refinement cycles prior to adding H atoms to the model.

The electron-density map for the active-site-bound ligand was of excellent quality, allowing us to model pepstatin A with full occupancy (Fig. 1*b*).

The atomic resolution achieved for the Sapp2 structure allowed the localization of numerous H atoms in the difference density maps and thus uncovered hydrogen-bonding networks. An example depicted in Fig. 2 shows part of the stabilizing hydrogen-bonding network of the flap closing over the active site and the hydrogen-bonding network leading to the catalytic residue. The side chain of Tyr77, a residue located next to the tip of the flap (Asp79), interacts with Trp39 through its O^{η} atom *via* a hydrogen bond to $H^{\varepsilon 1}$ of Trp39. The H^{η} atom of Tyr77 interacts with the O atom of water molecule 35 (Wat35). Wat35 donates one of its H atoms to a hydrogen bond to the main-chain carbonyl O atom of Asp37 and the second hydrogen to a hydrogen bond to the side-chain hydroxyl O atom (O^{γ}) of Ser35. H^{γ} of Ser35 donates a hydrogen bond to the $O^{\delta 2}$ atom of the catalytic residue Asp32. This hydrogen bond is critical for positioning the carboxyl group of Asp32 in a plane with the carboxyl group of the second catalytic residue Asp211 (see Fig. 6*a*). The positions of these H atoms are indicated by the presence of positive electron density (Fig. 2). Moreover, these densities are perfectly located between the hydrogen-bond acceptor and donor atoms.

3.3. Comparison of Sapp2p with related structures

The overall fold and topology of Sapp2p is similar to those of the other Sap family enzymes. The closest sequence and structural homologue of Sapp2p is Sapp1p. The sequence homology of these two isoenzymes is over 80% and their structures superpose with a root-mean-square deviation (r.m.s.d.) of 1.25 Å for 330 aligned C^{α} atoms (Fig. 3). Among the Saps from *C. albicans*, the most similar to Sapp2p in sequence and structure is Sap1 (sequence homology of 48%, r.m.s.d. of 2.64 Å for superposition of 331 aligned C^{α} atoms).

Both Sapp1p and Sapp2p contain two pairs of cysteine residues, and the S–S bridge topology is similar in both proteins (Cys47–Cys53 and Cys258–Cys292 in Sapp1p; Cys47–Cys52 and Cys249–Cys283 in Sapp2p). In addition, both the Sapp1p and Sapp2p isoenzymes contain one serine residue (Ser193 in Sapp1p and Ser184 in Sapp2p) encoded by the ambiguous CUG codon. These serines occur within loops (Leu182–Leu188 in Sapp2p; Val191–Thr198 in Sapp1p) that are topologically similar in both isoenzymes, although their sequence homology is quite low.

Despite the high structural similarity, there are noticeable differences between Sapp2p and Sapp1p. The major differences in backbone superposition between Sapp1p and Sapp2p are located in the loops that line the entrance to the substrate-binding cleft. There are two major differences in the entrance

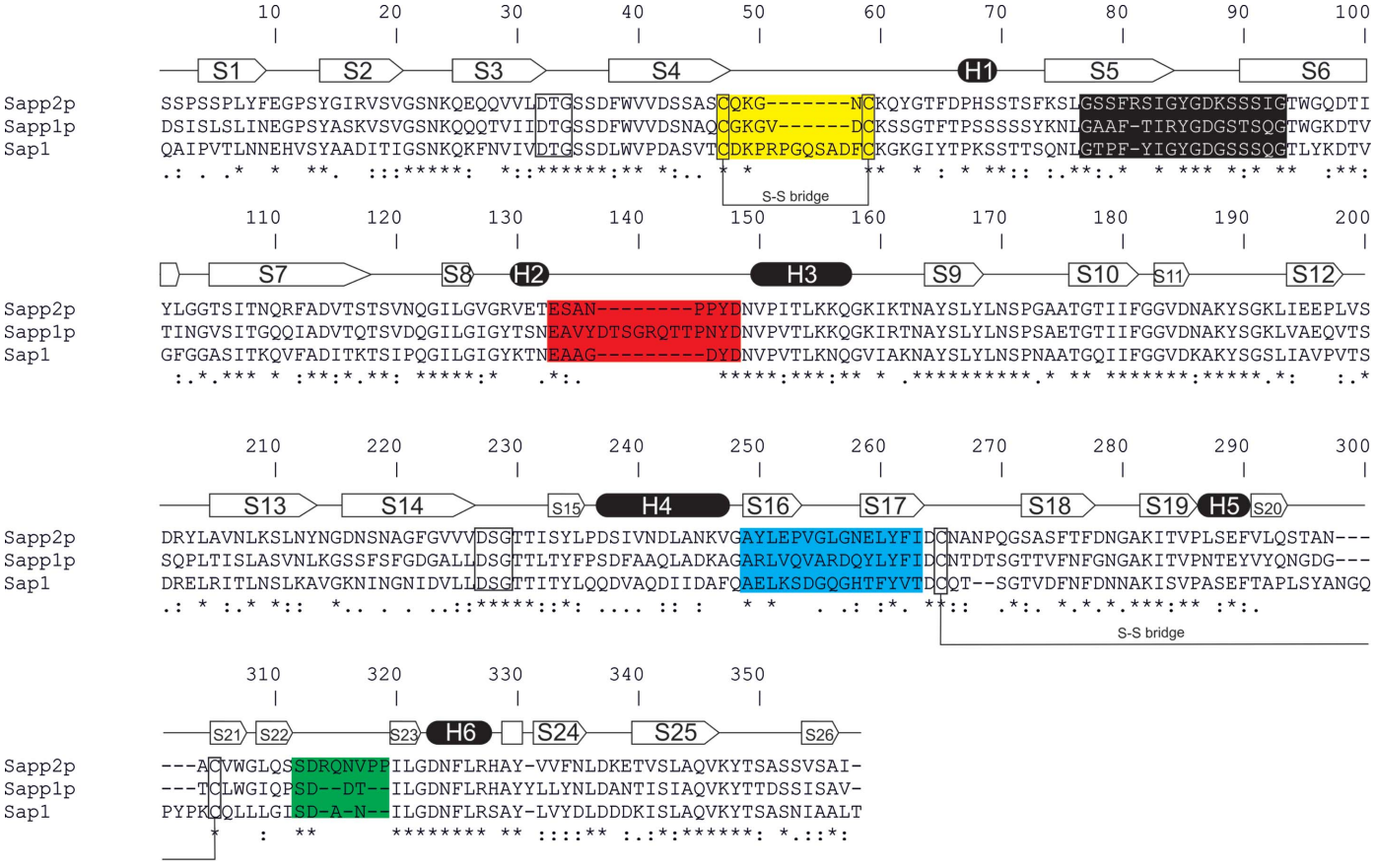

(*a*)

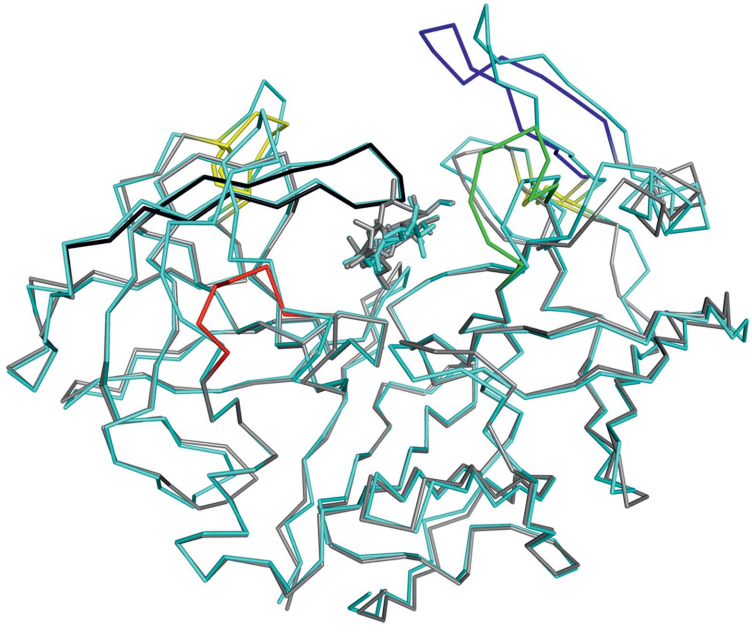

(*b*)

Figure 3
Comparison of Sapp2p with the homologous proteins Sapp1p (*C. parapsilosis*) and Sap1 (*C. albicans*). (*a*) Sequence alignment of Sapp2p, Sapp1p and Sap1. Secondary-structure elements (H, helices; S, strands) found in Sapp2p are shown. Identity is indicated by an asterisk (*), strong similarity is indicated by a colon (:) and weak similarity is indicated by a point (.). The residues of the active site are framed and the S–S bridges are indicated. The entrance-loop sequences are coloured as follows: N-ent loop 1, yellow; N-ent loop 2, red; C-ent loop 1, blue; C-ent loop 2, green. The flap region (Gly78–Gly104) is coloured black. (*b*) Superposition of the crystal structures of Sapp1p and Sapp2p in complex with pepstatin A. Sapp1p in complex with pepstatin A (PDB entry 3fv3; Dostál *et al.*, 2009) is coloured cyan. Sapp2p in complex with pepstatin A (PDB entry 4y9w; this work) is coloured grey with highlighted entrance loops and flap; the colour coding corresponds to that in (*a*). Pepstatin A is shown in stick representation and the S–S bridges are indicated as yellow sticks.

loops: a deletion in the Sapp2p sequence in N-ent loop 2 and an insertion in C-ent loop 2 of Sapp2p (Figs. 1 and 3). These loops are in direct contact with the C-terminal residue of pepstatin A, and their conformations significantly affect the character, shape and size of the substrate-binding cleft (Fig. 4).

Compared with Sapp1p, Sapp2p contains a deletion of eight amino acids in N-ent loop 2, resulting in the substrate-binding cleft being more open than that of Sapp1p. On the other hand, an amino-acid insertion in C-ent loop 1 of Sapp2p results in closure of the binding cavity, with a tighter embrace of the central part of the substrate/inhibitor (Fig. 4). Tight closing of the substrate-binding cleft of Sapp2p is mediated by interaction between the C-ent loops (residues Gln293, Val295 and Asn242) and the flap (residues Gly78 and Lys80).

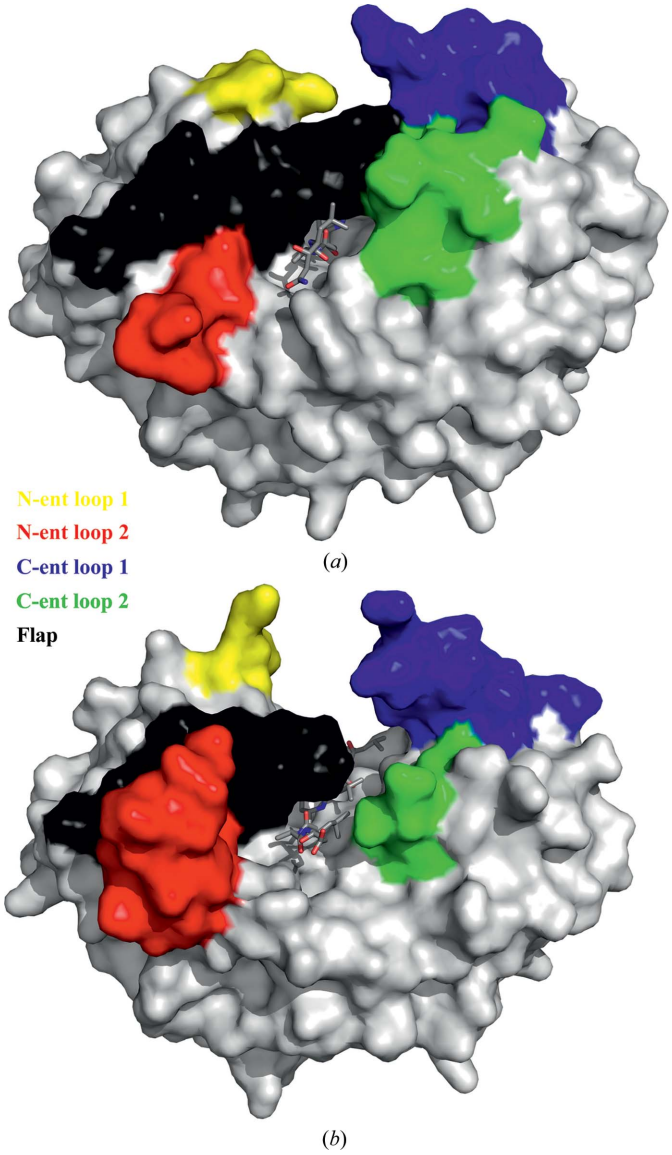

Figure 4
Overall structures of Sapp2p (*a*) and Sapp1p (*b*) represented by solvent-accessible surfaces. N-ent loop 1 and N-ent loop 2 are coloured yellow and red, respectively. C-ent loop 1 and C-ent loop 2 are coloured blue and green, respectively. The flap is coloured black and pepstatin A is shown in stick representation.

3.4. Pepstatin A binding to Sapp2p substrate-binding pockets

The active site, which is located between the two domains of the molecule at the bottom of a large cleft, is one of the most highly conserved regions in the Sap family. Pepstatin A, a peptide-like inhibitor containing six amino-acid residues in positions P4–P3′ (Iva1-Val2-Val3-Sta4-Ala5-StaOH6), bound to Sapp2p in an extended conformation, occupying the S4–S3 substrate-binding pockets of the active site of the enzyme. The pepstatin A conformation in Sapp2p is very similar to that observed in the previously reported structure of Sapp1p (Fig. 5*a*), with the exception of the Sta6 residue in position P3′. In the Sapp1p crystal structure, two alternative conformations of the Sta6 residue were observed (denoted I and II).

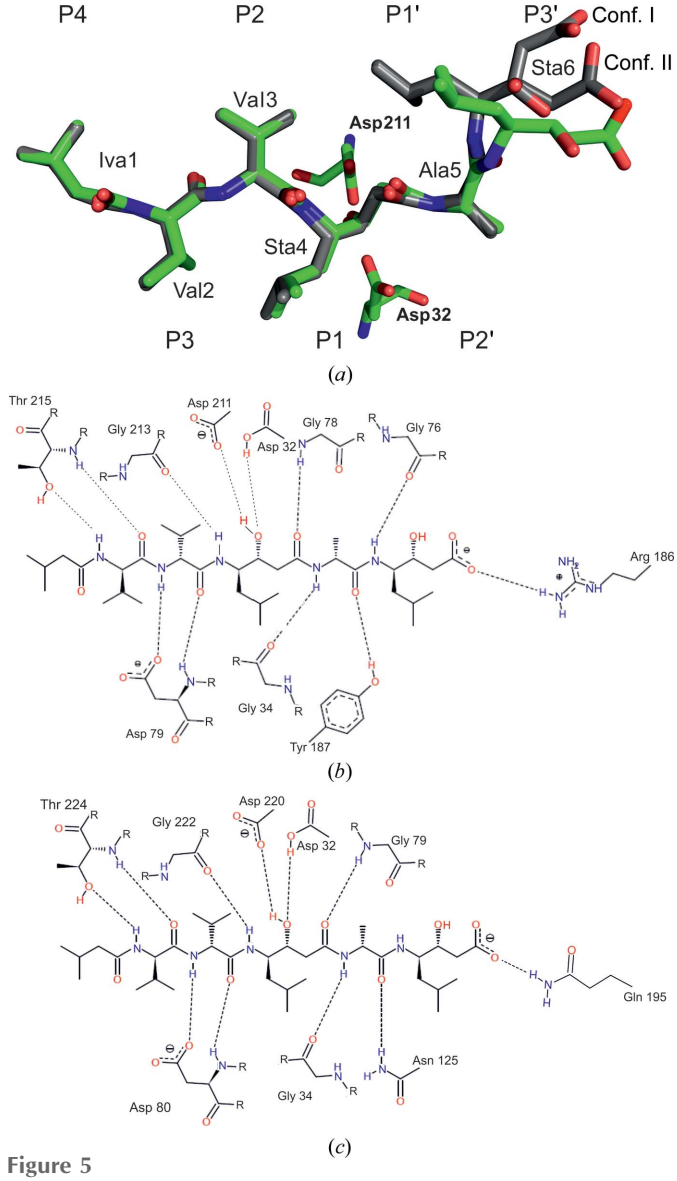

Figure 5
Pepstatin A binding to Sapp2p and Sapp1p. (*a*) Superposition of pepstatin A bound to Sapp2p (green C atoms) and Sapp1p in conformations I and II (grey C atoms). Two catalytic aspartates of Sapp2p are also depicted. O and N atoms are coloured red and blue, respectively. Schematic representations of hydrogen-bonding interactions of pepstatin A with the protein atoms of Sapp2p (*b*) and Sapp1p (*c*) are shown.

Table 2
Residues in contact (<4.2 Å) with pepstatin A in the Sapp1p and Sapp2p structures.

Residues that form hydrogen bonds to pepstatin A are shown in bold.

Subsite	Sapp2p	Sapp1p
S4	**Thr215**	**Thr224**
	Ile216	Leu225
	Tyr218	Tyr227
	Leu276	Tyr285
	Val284	Leu293
S3	Pro12	Pro12
	Ser13	
	Asp79	**Asp80**
	Gly213	**Gly222**
	Thr215	Thr224
S2	Tyr77	Tyr78
	Gly78	**Gly79**
	Asp79	**Asp80**
	Thr214	Thr223
	Tyr218	Tyr227
	Val295	
	Ile298	Ile303
S1	Val30	Ile30
	Asp32	**Asp32**
	Gly34	Gly34
	Tyr77	Tyr78
	Gly78	Gly79
	Asp79	Asp80
	Ser81	Ser82
	Ile116	Ile117
	Asp211	
	Gly213	Gly222
	Thr214	Ile303
S1′	**Gly34**	**Gly34**
	Gly76	
	Tyr187	**Asn125**
		Leu218
		Asp220
	Ile298	Ile303
S2′	Ser35	Ser35
	Ile75	Ile76
	Gly76	Gly79†
	Gly78	
	Arg186	Leu218†
	Tyr187	**Asn125**
S3′	Arg186	
		Gly79‡
		Gln195‡
		Asp301‡

† Residues interacting with pepstatin A conformation I. ‡ Residues interacting with pepstatin A conformation II.

The r.m.s.d.s for superposition of pepstatin A atoms bound to Sapp2p and Sapp1p are 1.06 and 1.47 Å for conformations I and II, respectively. When the first five residues of pepstatin A are compared, the r.m.s.d.s are 0.46 and 0.49 Å for conformations I and II, respectively. The structurally different binding of pepstatin A in Sapp2p compared with Sapp1p (Fig. 5*a*) is the result of three changes in the hydrogen bonding of the P2′ and P3′ inhibitor moieties (Fig. 5).

The side chain of the P4 residue Iva1 points towards the opening of the active site. The S3 and S2 subsites are occupied by Val2 and Val3, respectively. The side chain of Sta4 in the P1 position is closely packed against the side chain of Val2 in the P3 position. The Sta4 hydroxyl group is engaged in hydrogen-bonding interactions with the catalytic aspartates Asp32 and Asp211. Interestingly, the S1′ subsite is not occupied by the residue immediately following the P1 Sta4 but by a backwards-turned Sta6 side chain owing to a shift of register caused by the longer backbone of the statin moiety. The P2′ subsite is occupied by Ala5, which follows the P1 Sta4 in the sequence (Fig. 5*a*). The inverse γ-turn involving both Sta4 and Sta6 changes the direction of the inhibitor chain, leading the carboxylate of Sta6 towards the protein surface and occupying the S3′ subsite. As a result, the backbones of the P2′ Ala5 and the P3′ Sta6 residues deviate from the regular extended conformation. The different conformations of the P3′ Sta6 when bound to Sapp2p and Sapp1p, respectively, are caused by differences in the structure of the entrance to the active site, namely N-ent loop 2 and C-ent loop 1 (Fig. 4).

3.5. Polar and van der Waals interactions of pepstatin A with Sapp2p and Sapp1p

Direct hydrogen bonds to Sap isoenzymes are only supplied by the pepstatin A backbone (Figs. 5*b* and 5*c*). There are 12/11 direct hydrogen bonds between pepstatin A and Sapp1p/Sapp1p, respectively. Furthermore, the polar atoms of the P4 and P3′ residues are involved in water networks that help to hold the inhibitor in the enzyme cavity. Pepstatin A forms analogous hydrogen bonds to the Sapp2p and Sapp1p isoenzymes, with the following exceptions: (i) the carbonyl O atom of the P2′ Ala accepts a hydrogen from the phenolic hydroxyl of Tyr187 of Sapp2p but from the amide NH2 group of Asn125 in Sapp1p, (ii) the hydrogen donated by the NH group of Sta6 to Gly76 in Sapp2p is lost in Sapp1p owing to the presence of the bulky Arg77 side chain and (iii) the terminal carboxylate of Sta6 accepts a hydrogen bond from Arg186 of Sapp2p but from Gln195 in conformation II of Sapp1p (no hydrogen bond is formed in conformation I) (Figs. 5*b* and 5*c*).

The first difference (Tyr187/Asn125 in the S2′ pocket) creates an energy difference of up to 9 kcal mol^{-1} (see Fig. 7) that will partially be offset by the second difference (the presence and absence of Gly76). The third difference (Arg186/Gln195 in the S3′ pocket) favours Sapp2p binding by approximately 1 kcal mol^{-1}. An additional hydrogen bond (pepstatin A to Asp79 in Sapp2p or Asp80 in Sapp1p) appears to be structurally conserved but presents an energy difference of 3–4 kcal mol^{-1} in favour of Sapp1p. Additional calculations showed that this can be ascribed to a markedly more positive charge in the surroundings (Lys49 and Lys80) in Sapp2p. Furthermore, differences in the stabilization of the surrounding water cluster may come into play. Although the interactions of pepstatin A with Sapp2p and Sapp1p are mostly similar, we noted several mutually compensating differences, in line with the similar values of the measured inhibition constants of 0.4 and 0.3 n*M*, respectively, for the binding of pepstatin A to Sapp2p and Sapp1p.

In addition to polar interactions, pepstatin A makes numerous van der Waals interactions with the residues listed in Table 2. We carried out computational analysis of pepstatin A binding to the Sapp isoenzymes to assess the energy contributions of individual residue side chains (see §3.7).

3.6. Catalytic site protonation

The high resolution of our Sapp2p–pepstatin A structure and the low e.s.d. of the bond lengths (on the subpicometre scale) allowed us to suggest the protonation states of the catalytic aspartates (Fig. 6*a*). By comparing the distances between C^{γ} and $O^{\delta1/2}$ of catalytic aspartates with the optimal distances for a C—O single bond (1.3 Å) and a C═O double bond (1.2 Å), we identified which O^{δ} atoms are protonated (Wlodawer *et al.*, 2001). Moreover, the position of the Sta4 hydroxyl H atom, which mimics the transition state, is clearly visible in the difference electron-density map contoured at the 2σ level (Fig. 6*b*). The C—O interatomic distances in Asp211 indicate protonation of the $O^{\delta2}$ atom. The situation is slightly more complicated for Asp32 because the C—O distances in the carboxylic moiety are very similar (1.24 and 1.27 Å). The crystal structure is likely to reflect a superposition of two states: one in which both O^{δ} atoms are deprotonated (the optimal distance for a delocalized C—O partial double bond is 1.249 Å) and a minor form in which $O^{\delta1}$ is protonated. The occupancies of these two states were estimated to be 60 and 40%, respectively, based on the C—$O^{\delta1}$ distance.

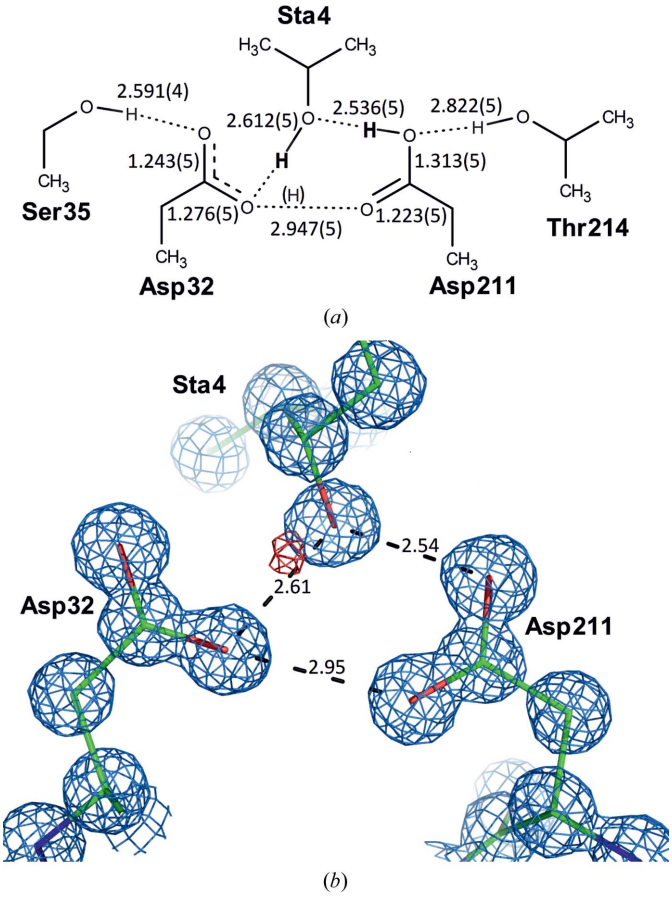

Figure 6
Polar interactions in the active site of the atomic resolution Sapp2p structure. (*a*) Schematic diagram with bonding distances (values are in Å; estimated standard deviations of distances are in parentheses). H atoms in bold are clearly assigned (the hydroxyl H atom of pepstatin was visible in difference electron density; the H atom on the protonated carboxyl of Asp211 was deciphered from C—O bonding distances). The H atom in parentheses is hypothetical. (*b*) Detailed structure of the active site in stick representation; hydrogen bonds are shown as dotted lines (numbers represent distances in Å). The $2F_o - F_c$ electron-density map contoured at the 1.5σ level is shown in light blue; the $F_o - F_c$ difference electron-density map contoured at the 2σ level is shown in red.

Protonation of Asp32 $O^{\delta1}$ can be achieved *via* the presence of the proton shared between the $O^{\delta1}$ atoms of the two catalytic aspartates or by a transient shift of the Sta4 hydroxyl H atom towards Asp32 $O^{\delta1}$. Proton sharing between the $O^{\delta1}$ atoms of two catalytic aspartates has been observed for a related aspartic protease, HIV-1 protease, in complex with a norstatine-based inhibitor (Brynda *et al.*, 2004). However, we found that a shared proton cannot be accommodated in the Sapp2p active site for steric reasons (the position of this hypothetical proton is shown in parentheses in Fig. 6*a*). Moreover, the shared-proton arrangement has far less favourable interaction energy with the statin inhibitor than the model with only two protons in the active site. We therefore suggest that the protonated state of Asp32 may indicate a transient shift of the statin hydroxyl proton towards $O^{\delta1}$ of Asp32.

The arrangement of the Sapp2p active site in our structure is very similar to the structures of other aspartic proteases in complex with an inhibitor with a hydroxyl group located between the active-site aspartates, such as the structures of endothiapepsin from the fungus *Endothia parasitica* (Coates *et al.*, 2002) and HIV-1 protease (Adachi *et al.*, 2009). In all of these atomic resolution X-ray structures, a proton is shared between the hydroxyl O atom of the inhibitor and the $O^{\delta1}$ atom of the catalytic aspartate.

3.7. Comparison of pepstatin A interactions with Sapp2p and Sapp1p

The residues involved in pepstatin A binding in Sapp2p and Sapp1p and the hydrogen-bonding pattern for the central binding pocket (S3–S1′) are mostly conserved (Figs. 5*b* and 5*c*). Most of the amino acids (75%) that form the Sapp1p and Sapp2p substrate-binding sites are conserved. Only residues involved in pepstatin A binding in the S2′ and S3′ subsites are significantly different between Sapp1p and Sapp2p. We used a virtual glycine scan (Pecina *et al.*, 2013) to study the roles of individual amino-acid side chains in the Sapp2p and Sapp1p active sites in the binding of pepstatin A. We used a fast and reliable semi-empirical quantum-mechanical (QM) method, PM6-D3H4X (Lepšík *et al.*, 2013). We needed a QM approach to quantitatively describe the strength of noncovalent interactions (Riley *et al.*, 2010), including quantum effects such as proton transfer. At the same time, using the semi-empirical approximation, we were able to include over 1000 atoms in the QM part and thus capture the long-range effects, such as electrostatic interactions.

The changes in the free energy of interaction ($\Delta\Delta G'_{\rm int}$) upon the mutation of a given amino-acid residue to glycine are shown in Fig. 7.

The amino-acid residues in the individual substrate-binding subsites of Sapp2p and Sapp1p fell into one of four categories: (i) identical residues, (ii) similar residues, (iii) different

residues and (iv) residues that do not form corresponding pairs owing to different tracing of the protein backbone. A fourth category comprises residues that do not form corresponding pairs owing to different tracing of the protein backbone. It is worth mentioning that the energy contributions inherently contain the effect of hydrogen bonding mediated by the residue side chain. The contributions of glycine residues (Gly213/Gly222 in S1, Gly78/Gly79 in S1/S1′ and Gly34/Gly34 in S1′) cannot be evaluated by the virtual glycine-scanning method. However, the contributions of these residues are likely to be very similar in Sapp2p and Sapp1p because they have similar conformations in both isoforms. The only exception in this category is the Gly76···Sta6 hydrogen bond, which is present in Sapp2p and absent in Sapp1p.

In the S4 subsite, we identified the following Sapp2p/Sapp1p residue pairs in the three categories defined above: (i) Pro12/Pro12 (also contributing to S3), Thr215/Thr224 (also contributing to S3) and Tyr218/Tyr227 (also contributing to S2); (ii) Ile216/Leu225 and Val284/Leu293; and (iii) Leu276/Tyr285. All of these pairs feature similar energy contributions within a difference of approximately 1 kcal mol^{-1}, even in category (iii) (Fig. 7). The strongest contribution to binding, of around 7 kcal mol^{-1}, is mediated by Thr215/Thr224. This is achieved by a combination of aliphatic···aliphatic interactions in the S4 subsite and hydrogen bonding in the S3 subsite.

The S3 subsite is relatively solvent-exposed. The only interacting residue in Sapp2p and Sapp1p is Ser13, which makes an almost identical contribution to the interaction energy in both enzymes (of close to 2 kcal mol^{-1}).

The S2 subsite is formed by several Sapp2p/Sapp1p conserved residues in category (i), Thr214/Thr223, Tyr218/Tyr227, Ile298/Ile303 (S2/S1′) and Asp79/Asp80 (S2/S1), and by Val296 of Sapp2p, which has no counterpart in Sapp1p. The conserved residues have similar contributions in Sapp2p and Sapp1p. Thr214/Thr223 has very strong interactions (around 7 kcal mol^{-1}) owing to a combination of aliphatic···aliphatic dispersion interactions in the S2 pocket and hydrogen bonding in the S1 pocket. Ile298/Ile303 has very weak (0.5 kcal mol^{-1}) methyl···methyl dispersion interactions (Jurecka *et al.*, 2006) in S2 that are identical for both enzyme isoforms. The contribution of this residue is, however, different in S1′. Interestingly, the conserved Asp79/Asp80 residue with an identical interaction pattern (two hydrogen bonds and a van der Waals interaction) has a difference of 3–4 kcal mol^{-1} in the energy of binding of pepstatin A to Sapp2p and Sapp1p, respectively. This difference can be ascribed to the long-range electrostatic influence of Lys49 and Lys80, which are present only in Sapp2p and are located approximately 7 Å from the charged Asp79 side chain. Additional interaction in the Sapp2p S2 subsite is mediated by Val296, which is located in the C-ent loop insertion and has no counterpart in Sapp1p.

The S1 subsite features the following Sapp2p/Sapp1p residues: (i) Ile116/Ile117, Tyr77/Tyr78 and Ser81/Ser82, and (ii) Val30/Ile30. All of these interacting residues provide similar contributions in Sapp2p and Sapp1p. Tyr77/Tyr78 provides a very large contribution of almost 9 kcal mol^{-1} owing to main-chain/main-chain hydrogen bonding combined with CH···π interactions.

The P1′ side chain of the Sta6 residue of pepstatin A features one nonpolar interaction of aliphatic···aliphatic type with the Pro296 side chain of Sapp2p. As this residue is located in the C-ent loop insert, Sapp1p does not have a counterpart. However, owing to the different pose of the P1′ moiety in Sapp1p there is a favourable interaction with Leu218. The Ile298/Ile303 pair only has interactions in Sapp1p.

In the S2′ subsite, there are the following Sapp2p/Sapp1p interacting residues: (i) Ile75/Ile76 and Ser35/Ser35 and (iii) Tyr187/Asn125. While the former two interact with pepstatin A only weakly, Tyr187 makes the strongest contribution to the energy of binding among all of the calculated interactions. The reason is a very short hydrogen bond (O···O distance of 2.6 Å) between the phenolic hydroxyl of Tyr187 and the backbone carbonyl of the Ala in P2′. Moreover, the Tyr187 Cζ···Oη bond length of 1.337 (9) Å suggests that the proton is shared between the two O atoms. In Sapp1p, however, interaction with the carbonyl of the Ala in P2′ is mediated by a medium-strong hydrogen bond to Asn125.

The P3′ terminal carboxylate of pepstatin A Sta6 is exposed to the solvent. In addition to hydrogen bonds to water molecules, it forms a salt bridge with Arg186 in Sapp2p, which is functionally

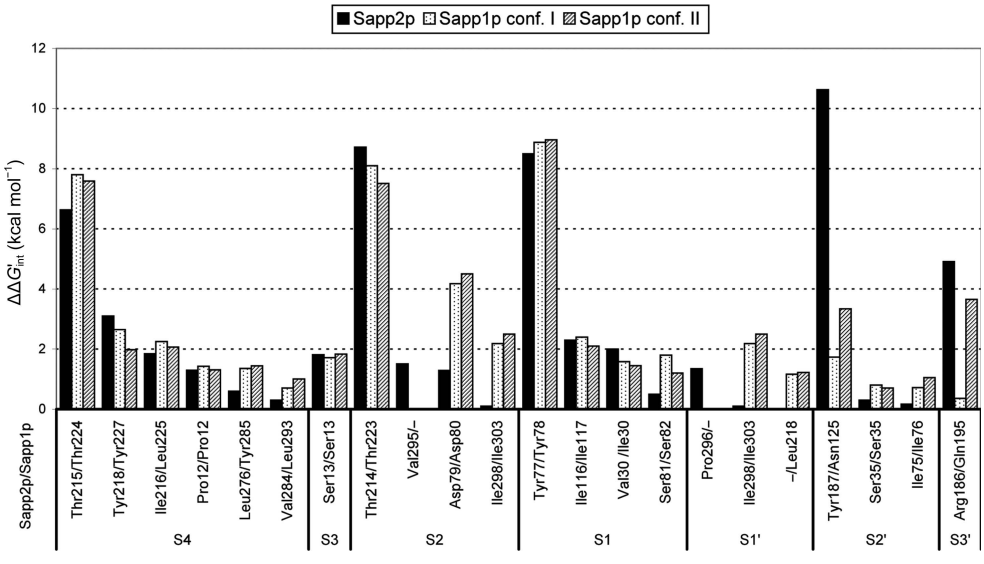

Figure 7
Energy contributions (kcal mol^{-1}) of the amino acids in Sapp2p and Sapp1p (two conformations of pepstatin A, I and II, were evaluated; *cf.* Fig. 5*a*) from a virtual glycine scan.

replaced in Sapp1p in conformation II by a charge-assisted hydrogen bond to Gln195.

Overall, our quantification of pepstatin A interactions with the Sapp2p and Sapp1p isoenzymes yielded similar results ($\sim$60 kcal mol^{-1} for Sapp2p and $\sim$55 kcal mol^{-1} for Sapp1p). This is the result either of similar interaction strengths or some weaker and other compensating stronger interactions. Our finding is in line with the similar values of the measured inhibition constants of 0.4 and 0.3 n*M*, respectively, for the binding of pepstatin A to Sapp2p and Sapp1p.

In summary, we have analyzed the binding of pepstatin A to the Sapp2p and Sapp1p isoenzymes by a combination of high-resolution crystallography and advanced quantum-chemical interaction energy calculations.

Acknowledgements

This work was supported by grant GA14-23022S from the Czech Science Foundation and by projects RVO 61388963 and RVO 68378050 awarded by the Academy of Sciences of the Czech Republic. The research leading to these results has received funding from the European Community's Seventh Framework Programme under BioStruct-X (grant agreement No. 283570). The authors would like to thank the IOCB MS facility for performing the peptide mass-fingerprinting analysis and Elena Dolejší for technical assistance.

References

Abad-Zapatero, C., Goldman, R., Muchmore, S. W., Hutchins, C., Stewart, K., Navaza, J., Payne, C. D. & Ray, T. L. (1996). *Protein Sci.* **5**, 640–652.
Adachi, M. *et al.* (2009). *Proc. Natl Acad. Sci. USA*, **106**, 4641–4646.
Bayly, C. I., Cieplak, P., Cornell, W. D. & Kollman, P. A. (1993). *J. Phys. Chem.* **97**, 10269–10280.
Berendsen, H. J. C., Postma, J. P. M., van Gunsteren, W. F., DiNola, A. & Haak, J. R. (1984). *J. Chem. Phys.* **81**, 3684–3690.
Bitzek, E., Koskinen, P., Gähler, F., Moseler, M. & Gumbsch, P. (2006). *Phys. Rev. Lett.* **97**, 170201.
Borelli, C., Ruge, E., Lee, J. H., Schaller, M., Vogelsang, A., Monod, M., Korting, H. C., Huber, R. & Maskos, K. (2008). *Proteins*, **72**, 1308–1319.
Borelli, C., Ruge, E., Schaller, M., Monod, M., Korting, H. C., Huber, R. & Maskos, K. (2007). *Proteins*, **68**, 738–748.
Brynda, J., Rezacova, P., Fabry, M., Horejsi, M., Stouracova, R., Sedlacek, J., Soucek, M., Hradilek, M., Lepsik, M. & Konvalinka, J. (2004). *J. Med. Chem.* **47**, 2030–2036.
Case, D. A. *et al.* (2008). *AMBER* 10. University of California, San Francisco.
Coates, L., Erskine, P. T., Crump, M. P., Wood, S. P. & Cooper, J. B. (2002). *J. Mol. Biol.* **318**, 1405–1415.
Cutfield, S. M., Dodson, E. J., Anderson, B. F., Moody, P. C., Marshall, C. J., Sullivan, P. A. & Cutfield, J. F. (1995). *Structure*, **3**, 1261–1271.
Diederichs, K. (2010). *Acta Cryst.* D**66**, 733–740.
Dostál, J., Brynda, J., Hrušková-Heidingsfeldová, O., Pachl, P., Pichová, I. & Řezáčová, P. (2012). *J. Enzyme Inhib. Med. Chem.* **27**, 160–165.
Dostál, J., Brynda, J., Hrušková-Heidingsfeldová, O., Sieglová, I., Pichová, I. & Řezáčová, P. (2009). *J. Struct. Biol.* **167**, 145–152.
Dostál, J., Hamal, P., Pavlícková, L., Souček, M., Ruml, T., Pichová, I. & Hrusková-Heidingsfeldová, O. (2003). *J. Clin. Microbiol.* **41**, 712–716.
Dostál, J., Merkerová, M., Vinterová, Z., Pichová, I. & Hrušková-Heidingsfeldová, O. (2015). *Folia Microbiol. (Praha)*, **60**, 373–374.
Duan, Y., Wu, C., Chowdhury, S., Lee, M. C., Xiong, G., Zhang, W., Yang, R., Cieplak, P., Luo, R., Lee, T., Caldwell, J., Wang, J. & Kollman, P. (2003). *J. Comput. Chem.* **24**, 1999–2012.
Emsley, P. & Cowtan, K. (2004). *Acta Cryst.* D**60**, 2126–2132.
Fusek, M., Smith, E. A., Monod, M. & Foundling, S. I. (1993). *FEBS Lett.* **327**, 108–112.
Gruene, T., Hahn, H. W., Luebben, A. V., Meilleur, F. & Sheldrick, G. M. (2014). *J. Appl. Cryst.* **47**, 462–466.
Hrušková-Heidingsfeldová, O. (2008). *Front. Biosci.* **13**, 7227–7242.
Hrušková-Heidingsfeldová, O., Dostál, J., Majer, F., Havlíková, J., Hradilek, M. & Pichová, I. (2009). *Biol. Chem.* **390**, 259–268.
Hube, B. & Naglik, J. (2001). *Microbiology*, **147**, 1997–2005.
Jurecka, P., Sponer, J., Cerný, J. & Hobza, P. (2006). *Phys. Chem. Chem. Phys.* **8**, 1985–1993.
Kabsch, W. (2010). *Acta Cryst.* D**66**, 125–132.
Leibovitz, E., Livshiz-Riven, I., Borer, A., Taraboulos-Klein, T., Zamir, O., Shany, E., Melamed, R., Rimon, O. F., Bradenstein, R., Chodick, G. & Golan, A. (2013). *Scand. J. Infect. Dis.* **45**, 842–848.
Lepšík, M., Řezáč, J., Kolář, M., Pecina, A., Hobza, P. & Fanfrlík, J. (2013). *Chempluschem*, **78**, 921–931.
Merkerová, M., Dostál, J., Hradilek, M., Pichová, I. & Hruskova-Heidingsfeldova, O. (2006). *FEMS Yeast Res.* **6**, 1018–1026.
Mueller, U., Darowski, N., Fuchs, M. R., Förster, R., Hellmig, M., Paithankar, K. S., Pühringer, S., Steffien, M., Zocher, G. & Weiss, M. S. (2012). *J. Synchrotron Rad.* **19**, 442–449.
Naglik, J., Albrecht, A., Bader, O. & Hube, B. (2004). *Cell. Microbiol.* **6**, 915–926.
Pammi, M., Holland, L., Butler, G., Gacser, A. & Bliss, J. M. (2013). *Pediatr. Infect. Dis. J.* **32**, e206–e216.
Parra-Ortega, B., Cruz-Torres, H., Villa-Tanaca, L. & Hernández-Rodríguez, C. (2009). *Mem. Inst. Oswaldo Cruz*, **104**, 505–512.
Pecina, A., Lepšík, M., Řezáč, J., Brynda, J., Mader, P., Řezáčová, P., Hobza, P. & Fanfrlík, J. (2013). *J. Phys. Chem. B*, **117**, 16096–16104.
Pettersen, E. F., Goddard, T. D., Huang, C. C., Couch, G. S., Greenblatt, D. M., Meng, E. C. & Ferrin, T. E. (2004). *J. Comput. Chem.* **25**, 1605–1612.
Pfaller, M. A. *et al.* (2010). *Diagn. Microbiol. Infect. Dis.* **67**, 162–171.
Pichová, I., Pavlíčková, L., Dostál, J., Dolejší, E., Hrušková-Heidingsfeldová, O., Weber, J., Ruml, T. & Souček, M. (2001). *Eur. J. Biochem.* **268**, 2669–2677.
Pryszcz, L. P., Németh, T., Gácser, A. & Gabaldón, T. (2013). *Genome Biol. Evol.* **5**, 2382–2392.
Rao, J. K., Erickson, J. W. & Wlodawer, A. (1991). *Biochemistry*, **30**, 4663–4671.
Riley, K. E., Pitoňák, M., Jurečka, P. & Hobza, P. (2010). *Chem. Rev.* **110**, 5023–5063.
Trofa, D., Gácser, A. & Nosanchuk, J. D. (2008). *Clin. Microbiol. Rev.* **21**, 606–625.
Vagin, A. & Teplyakov, A. (2010). *Acta Cryst.* D**66**, 22–25.
Wang, J., Wolf, R. M., Caldwell, J. W., Kollman, P. A. & Case, D. A. (2004). *J. Comput. Chem.* **25**, 1157–1174.
Wlodawer, A., Li, M., Gustchina, A., Dauter, Z., Uchida, K., Oyama, H., Goldfarb, N. E., Dunn, B. M. & Oda, K. (2001). *Biochemistry*, **40**, 15602–15611.